International Journal of Engineering

Journal Homepage: www.ije.ir

The Comparison of Punching Shear Capacity in Solid and Void Two-Way Slabs on Soil Substrate in Relation to Spring Stiffness Changes

H. Azizian[a], M. A. Lotfollahi-Yaghin*[b], A. Behravesh[a]

[a] *Department of Civil Engineering, Mahabad Branch, Islamic Azad University, Mahabad, Iran*
[b] *Civil Engineering Faculty, University of Tabriz, Tabriz, Iran*

PAPER INFO

Paper history:
Received 02 May 2020
Received in revised form 05 July 2020
Accepted 04 August 2020

Keywords:
Laboratory Model
Numerical Model
Punching Shear Capacity
Soil and Spring Model
Spherical Plastic Hollow Formers
Two-Way Solid and Hollow Slabs

ABSTRACT

This study aims to investigate punching shear in solid and void slabs as well as simulated soil and spring models as distributed loads on the mentioned slabs. To this end, the slabs were tested using the nonlinear finite element analysis under static loading to assess their failure in terms of the final load and cracking patterns on the soil substrate and spring. For this purpose, a 3D finite element analysis was performed based on the element size, mesh, and concrete characteristic modeling. In Finite Element Software ABAQUS 6.19, the nonlinear behavior of brittle materials was defined based on the concrete damaged plasticity (CDP) model. Next, the results of the numerical analysis of the slabs were calibrated and validated based on a comparison with experimental specimens on a soil substrate. At the end, by optimizing the spring constant and obtaining the soil spring constant, the results of the numerical analysis of the slabs on the spring support were compared to the experimental results, which showed the calibrated models correctly predicted the punching cutting response of the slabs.

***doi**: 10.5829/ije.2020.33.10a.06*

NOMENCLATURE

f_c	Concrete Strength (MPa)	φ	Angle of Internal Friction of the Soil (degrees)
Ecm	Concrete Young's Modulus (GPa)	ψ	Effective angle of internal friction (degree)
f_t	Concrete Tensile Strength (MPa)	*R*	Solid slab
υ	Poisson's Ratio	S_1	Void slab
γ_c	Density of concrete (kg/m3)	h	The depth of slab (mm)
Es	Steel Young's Modulus (MPa)	d	The effective depth of slab = 100 mm
f_r	Reinforcement Tensile Strength (MPa)	P_1R_1	Point one slab R
γ	unit weight (mm)	P_1S_1	Point one slab one the depth of slab (mm)
E	Young's soil modulus (MPa)	Cc	Coefficient of curvature
σ	Pressure or stress (MPa)	Cu	Coeffi cient of uniformity
ε	Strain	D10	Grain sizes for which 10% of the soil grains are smaller
C	Cohesion of a soil	D30	Grain sizes for which 30% of the soil grains are smaller

1. INTRODUCTION

The first study on punching shear was conducted by a series of experiments on reinforced concrete foundations and also the interaction between the foundations and soil through steel springs was simulated. Later on, many researchers evaluated different methods of simulating soil-structure interactions. Employing a system driven by hydraulic cylinders to simulate a uniform load distributed over a foundation, their study was used as a reference work for future studies [1, 2], for instance testing slab-column fixtures by examining foundations with

*Corresponding Author, E-mails: *lotfollahi@tabrizu.ac.ir* (M. A. Lotfollahi-Yaghin)

Please cite this article as: H. Azizian, M. A. Lotfollahi-Yaghin, A. Behravesh, The Comparison of Punching Shear Capacity in Solid and Void Two-Way Slabs on Soil Substrate in Relation to Spring Stiffness Changes, International Journal of Engineering (IJE), IJE TRANSACTIONS A: Basics Vol. 33, No. 10, (October 2020) 1872-1885

uniformly distributed loading systems [3]. Punching investigation of the footing rested on real soil was done in practice only by using a sandbox test system to simulate soil effects and sand density, with the latter factor being a variable ranging from loose to dense [4–6]. Later on, similar experiments were conducted using a mixture of river sands [7]. Other studies were also carried out to investigate the punching shear of slabs [8]. Some experiments were conducted at the University of Pretoria in 2014, in which they used concrete slabs on 9 springs as supports and compared spring stiffness with soil stiffness [9, 10].

Analyses free vibration of a beam on elastic foundation by applying the variational iteration method (VIM) for three different axially loaded cases were adopted including one end clamped and the other end simply supported, both ends clamped, and both ends simply supported cases. In this paper, for different ratios of axial load acting on the beam to Euler buckling load, analytical solutions and frequency factors are evaluated. It is shown that the results obtained by VIM method in this paper are in compliance with the differential transform method (DTM) results for fixed-pinned case [10–14]. Also, homotopy perturbation method (HPM) was applied for free vibration of a beam on elastic foundation by Ozturk and Coskun [15]. In another research, analytical solutions for free vibration of a beam on elastic foundation were analyzed by Ozturk and Coskun [16] for the three cases considered above. Also, frequency factors were calculated for different ratios of axial load acting on the beam to Euler buckling load. The results obtained by the analytical solution are in good agreement with the_variational iteration method (VIM) results achieved in the previous research and homotopy perturbation method (HPM) results for three different axially loaded cases.

In reinforced concrete (RC) column footings, the soil stiffness can significantly affect the punching shear strength of the foundation slab. The present study conducted eccentric compression tests on three RC column footings considering the complex interaction between the soil and structure, and investigated the load-carrying capacity, displacement distribution, reaction distribution, failure mode, crack development, and strain distribution. However, column footings are generally subjected to eccentric compression. Thus, it is necessary to investigate the punching failure mechanism of column footings under eccentric compression. As the flexural reinforcement ratio increased, the observed critical angle of failure cone was increased from 44° to 54°. Such failure angle was steeper than that of flat slabs (30° to 45° when a/d = 3.22 to 8.80). The flexural reinforcement ratio affected the crack distribution area and the spalling of concrete cover [17].

By evaluating previous studies on punching shear, majority of the studies used simply support and concentrate load to the center of top face of slab, thus obtaining a punch shear. In this study, soil and spring have been used to simulate distributed load to obtain the punching shear capacity with low bending effect in two way bubble voided slabs. For a more accurate comparison, it was not possible to perform the spring test. In future research, it is possible to test such springs with the stiffness obtained from Abaqus software and to compare the soil and spring results.

However, in cases where the slab is placed on the soil support when applying the load to the column, if the soil is under the slab, the underside of the column itself will be completely rigid due to slight deformation occurring to the slab, which exhibits a high capacity that functions almost like a rigid wedge. In other words, the bottom of the column in the soil, with its relatively rigid performance, carries the main load of the column; thus, it could not be clear for which load the punching shear occurs. In addition, when one part of the column load is supported by the soil beneath the column and another part is loaded on other parts of the soil, it will not be practically detectable at the time of shear failure which simply occurs due to the area outside the cutting line. However, when the part under the foundation is emptied or replaced with low strength materials, most of the column load will be carried through the punching shear. In addition, when the slab undergoes failure, it will be determinable at which load the slab undergoes failure in the form of punching shear [10].

Furthermore, in cases where the slab is placed on the spring support when applying the load to the column, the area under the column will be displaced more than the areas around it. If the springs are placed beneath the column, they will impose heavier loads on the slab than farther springs, thereby preventing the slab from being displaced and thus preventing the area under the column from falling. This will, in turn, prevent slab failure, and the column springs will carry the main load of the column; hence, it could not be determined under which load the slab will undergo shear failure.

This paper is organized in three sections; in the first part, the punching shear capacity and the failure mechanism of the solid slabs were tested against two-way void slabs under the influence of a centralized load at the slab center, on the soil substrate, by the elimination of errors. Given that the application of the distributed load to the slab and the maintenance of column equilibrium in the laboratory analysis of slab punching require advanced devices and equipment, another method was adopted in this study for performing this experiment. For this purpose, the space under the slab column was emptied because slab thickness is relatively low in the laboratory, and the slab does not function totally as a rigid object. Thus, the space beneath the foundation is left empty by inserting a sponge until the error is reduced, and the net load leading to the punching shear failure of the slab is

calculated. In this manner, the slab and the column are inverted on a uniform granular soil substrate in the form of a surface foundation, and axial loading is applied to the column. In the second part, the laboratory specimens are simulated using Finite Element Software ABAQUS, and then the punching shear of the hollow and solid slabs on the soil substrate is examined. In the third part, the laboratory specimens are simulated using Finite Element Software ABAQUS, and the punching shear of the hollow and solid slabs on springs with different constants are investigated, i.e. the springs are modeled instead of uniformly distributed loads. To eliminate the errors and problems mentioned above, no spring should be placed under the area exposed to the punching shear. However, the best area that should be left empty (for both the soil substrate and the spring) is the region encompassing the column area in addition to d, i.e. effective slab thickness, provided that the location of the failure is exactly on a plate. However, this happens neither in practice nor in ABAQUS because the failure area has a significant width across which several elements reach the failure area simultaneously; thus, this area could be of variable widths. In the end, the experimental results are compared with those of the numerical analysis for the springs and the soil substrate.

2. EXPERIMENTAL STUDY

2. 1. Specimens and Materials In this study, a two-way solid slab (R) and a void slab (S_1) were used as reference specimens as shown in Figures 1 and 2. In the specimen, spherical hollow formers are arranged 100 mm away from the edge of the column. The dimensions of all slabs were 1300×1300 mm. Slab thickness and effective thickness were 120 mm and 100 mm, respectively. Slab slots were filled using traditional spherical plastic hollow formers. The diameter of the spherical plastic hollow formers was 70 mm in the designed layout, and the balls were arranged at 20 mm and 90 mm center-to-center distances, with these distances and scales set by a string as Figures 3a and 3b display. The slabs were made of plain concrete with the same mixing scheme as shown in Table 1. Given that in numerical modeling, the elastic and plastic behavior of concrete (CDP) as well as the rebar must be correctly inserted in ABAQUS software, it was required to test the mechanical properties of the concrete. To this end, 5 cylindrical specimens were produced and tested after 28 days (Figure 4a). The stress-strain curve of the concrete produced in the material tests showed that the average strength of the cylindrical specimen was 31.77 N/mm^2. Figure 4b shows the stress-strain curve of the concrete specimens where the average tensile strength of the concrete was 3.57 MPa for the 5 specimens. Table 2 summarizes the mechanical properties of the concrete.

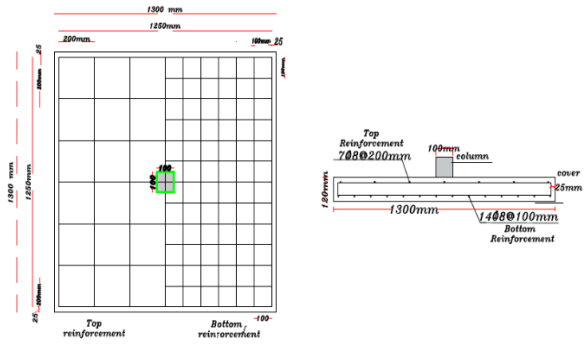

Figure 1. Double-sided solid slab R and the layout of bending bars in the specimens

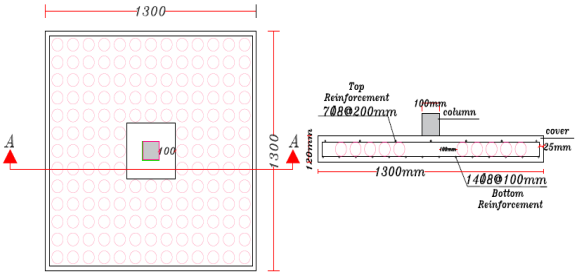

Figure 2. Implementation details of the balls in the S1 void slab specimen (dimensions in mm)

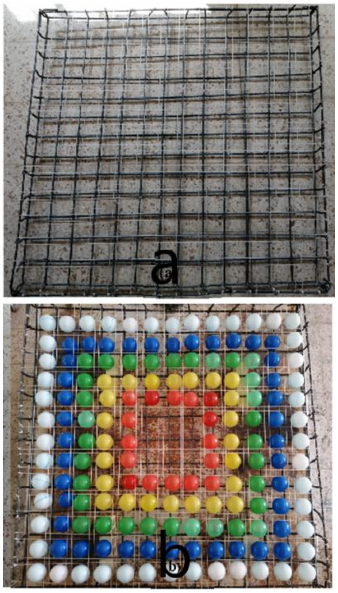

Figure 3. (a) The layout of bending bars in the specimens for determining spacing and scaling with the string, as well as (b) the S1 void slab specimen

TABLE 1. The concrete mixing design used for slabs Strouhal number for different geometric cases [12]

Water (kg/m^3)	Cement (kg/m^3)	Gravel (m^3)	Sand (m^3)	Slump (mm)
175.49	443	902	910	65

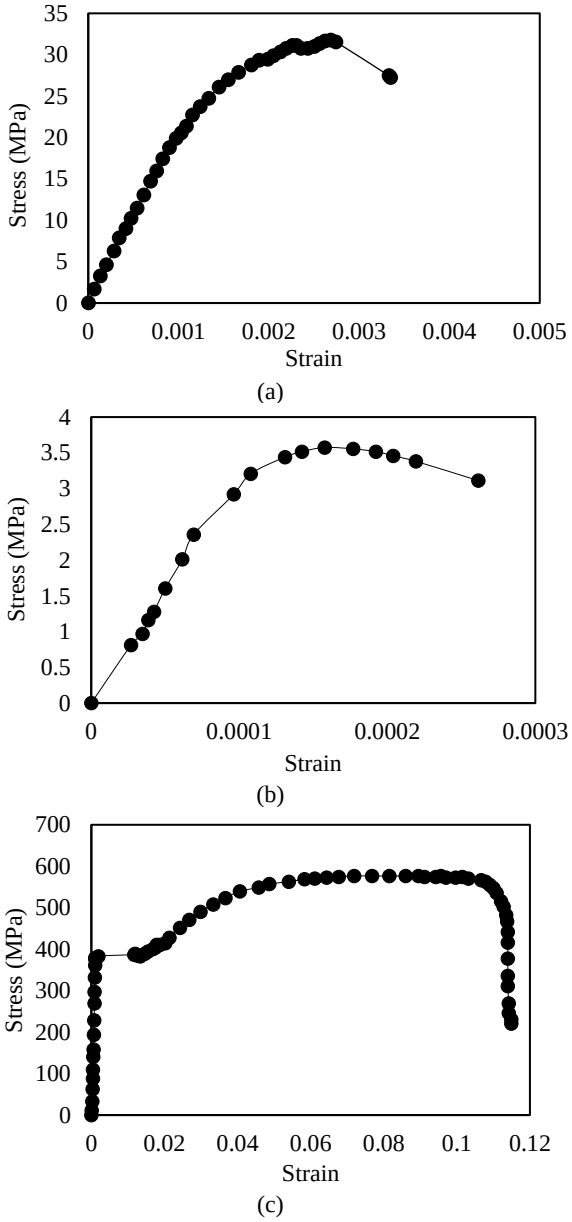

Figure 4. Material test results; (a) Concrete compressive strength; (b) Concrete tensile strength; (c) Rebar tensile strength

Figure 4c demonstrates the stress-strain curve of the rebar with D8 diameter, with the yield strength and tensile strength of 383.062 MPa and 576.547 MPa, respectively. The slabs were fitted with longitudinal and transverse steel bars. Table 3 lists the mechanical features of the test slab bars. The bars located at the bottom and top substrates were 8 mm in width [12].

The results of soil aggregation, classification properties, as well as plastic, elastic, and weight-volumetric parameters are presented as well. Mechanical soil aggregation was tested using the dry method, with the aggregation curve shown in Figure 5. Since

TABLE 2. Specifications of the concrete used in slab construction [12]

fc, MPa	Ecm, GPa	fr, MPa	υ	Density
31.77	25.47	3.57	0.15	2400

TABLE 3. Specifications of the rebar used in slab construction [12]

Diameter (mm)	Es, GPa	fr, MPa	υ	Density (kg/m^3)	Elo, (%)
8	201.45	576.54	0.3	7850	**17**

uniformity and curvature coefficients are Cu <6 and Cc <1 or Cc> 3, respectively, the soil is classified as SP, i.e. poorly graded. Direct shear tests were done to determine the plastic parameters (C and φ) of the soil specimen, with the results of which presented in Figure 6. Given that another parameter required in numerical modeling is the elastic modulus (E) of the soil, the loaded soil was used in a uniaxial test device to simulate soil natural conditions so as to determine the E value. Figure 7 demonstrates the stress-strain curve of the soil specimen, which is extracted based on the initial fitness slope of the stress-strain curve of the elastic modulus for the soil specimen.

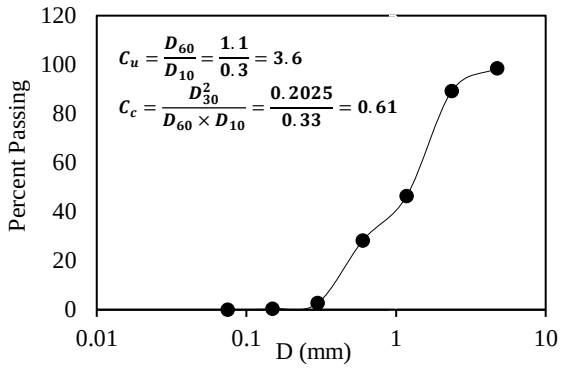

Figure 5. The grading curve

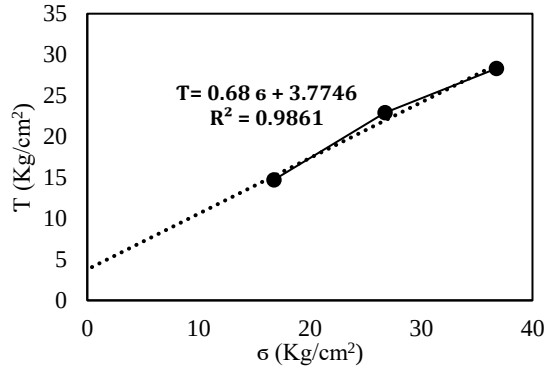

Figure 6. Fracture coverage obtained from direct shear test results

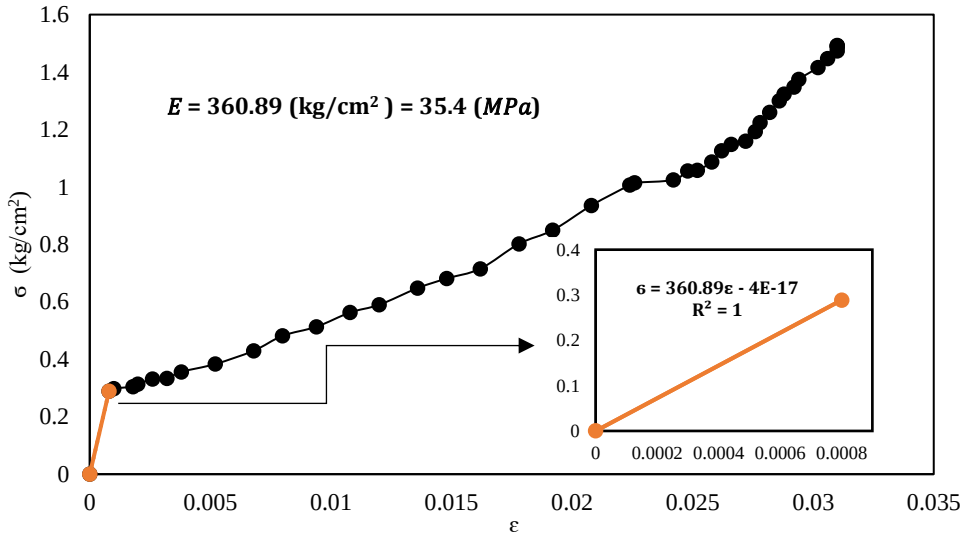

Figure 7. The stress-strain curve for the soil specimen

The value of the Poisson coefficient (ν) for the soil specimen (SP) ranged from 0.15 to 0.4 with an average of ν = 0.3. Tables 4 and 5 show the calculated values ofthe specific weight (γ) and the saturation specific weight (γ_sat) of the soil. Table 6 demonstrates the results of all soil engineering tests.

2. 2. The Laboratory Program First of all, a 370×340×340 mm sponge or a low resistance material was installed under the column in the middle of a 1300×1300×500 mm cubic steel box to minimize box deformation. Accordingly, the space under the slab column was left empty. Next, the box was filled with uniform granular soil up to 37 cm high, which reached the upper level of the sponge. As Figures 8 and 9 show, solid slab R and void slab S1 were placed on the soil substrate as the support. When applying the load, a 150×100×100 mm metal piece was used at the slab center to replace the column, as Figure 10 shows. As the column was rigid and did not undergo any deformations, it applied the jack load exactly to the slab. Accordingly, if the reference point was placed either on the slab, at the center of the column, on the top, or in the middle of the column, it would make no change to the results. Therefore, the column midpoint was considered the load-displacement reference point. A 200-ton hydraulic system, based at the Civil Engineering Laboratory and controlled by a computer system, was used for loading purposes. A linear variable differential transformer (LVDT) with a 100 mm course and 0.01mm accuracy was attached to the loading jaw, with the vertical

TABLE 4. Soil specific weight

W_1 (g)	W_2 (g)	V_i (cm^3)	W_i (g_r)	$\gamma_i = \frac{W_i}{V_i}$ ($\frac{KN}{m^3}$)
306	420	76.9	114	14.82

TABLE 5. Soil engineering specifications

E (Mpa)	υ	C (kN/m^2)	φ°	ψ°	ɣ	$ɣ_{sat}$
35. 4	0.3	3.77	34	4	14.82	18.72

TABLE 6. A comparison of experimental and numerical final loads for solid and void slab models

Slab Model Symbol	Ultimate Load Pu (kN)	Deflection (mm)	1st Crack Load P_{cr} (kN)	Difference Ratio %	Failure Mode
R	7.60	96.04	-	-	Punching shear
S_1	7.26	85.26	14.48	14.48	Punching shear

Figure 8. Test Setup [13]

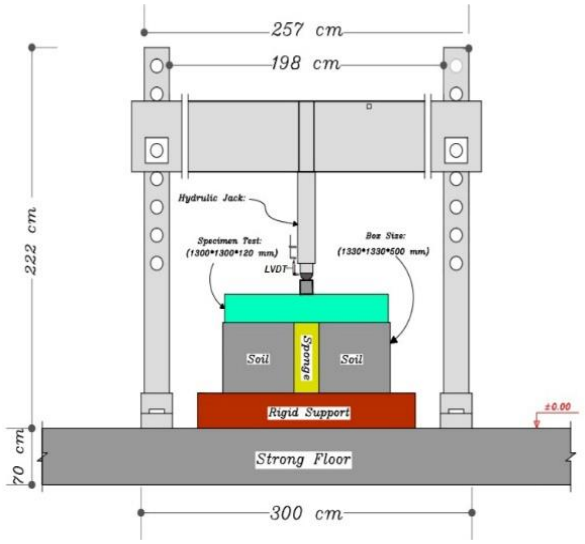

Figure 9. Schematic testing equipment

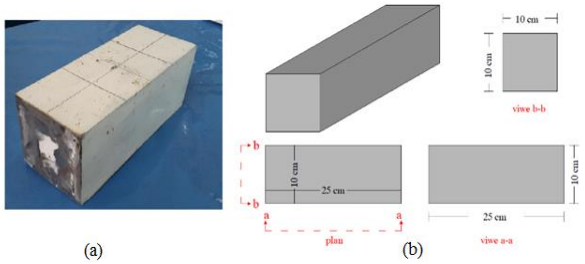

(a) (b)

Figure 10. Steel column specification

displacement of the slab surface midpoint measured during the experiment. The load applied to the column increased gradually by 1kN/s until the specimens were broken, and the load-displacement diagram failed abruptly. The load-displacement rate was automatically saved to the software installed on the computer [12].

2. 3. Experimental Results

2. 3. 1. Load-Deflection Results Upon applying the load to the center of the slab, the first cracks appeared in both specimens in the tensile area, near one or more corners of the column. Upon more loading, the number of cracks in the central area of the slab increased, and the slab stretched to its four edges. In fact, the first shear cracking of the solid and void slabs started upon applying the final loads (45.79% and 47.54%) (See Table 6). According to Figure 11, the load-deflection response curves of both laboratory specimens show elastoplastic behavior. Besides, the slope of the curves is approximately the same for both slabs because it depends on slab stiffness and the type of loads. The effect of spherical balls, in the void concrete slabs, on the final punching shear capacity was determined as well. As Table 6 presents, due to the presence of the void formers, the final loads applied to the void slabs were smaller than those applied to the solid slabs. In the meantime, the ductility of the void slabs was higher than that of the solid ones. The slabs underwent punching shear after reaching the final load. The shear failure of the specimens was measured abruptly for R and S1 slabs at the final loads of 209.72 and 179.34 kN, respectively, with the force decreased immediately after the specimen failed. The values of the punching shear capacity were different in these two slabs by about 14.48%. In addition, vertical deflection in the middle of the slabs, measured by the linear variable differential transformer (LVDT), was almost similar in both slabs. However, the deflection was not affected by the spherical void formers until the initial cracking.

2. 3. 2. The Slab Fracture Mechanism As it was mentioned earlier, after the final loading, the slabs were fractured through punching shear and carefully examined for the type and location of the developed cracks. Accordingly, it is noteworthy that the shape of the failure region was asymmetric even if the shape of the slab, rebar, and load was symmetric. Several cracks were developed in the lower surface of the slabs, as Figures (12a) to (13a) show, which demonstrate the final crack patterns of the slabs. The failure pattern occurred at the initial loading in the form of a partially oblique and pyramidal shape on the slab surface. Besides, the presence of the bending bars that increased the tensile capacity of the slab affected the failure angle, thereby extending the crack length from the slab middle point to the edge. Bending failure modes were observed in the two-way solid and void slabs with irregular elliptical shapes below the slabs. The irregular shape could be the result of the heterogeneity of the materials, including the concrete, the soil beneath it, and the existence of steel bars. However, there were no cracks on the slab surface visible to the naked eye.

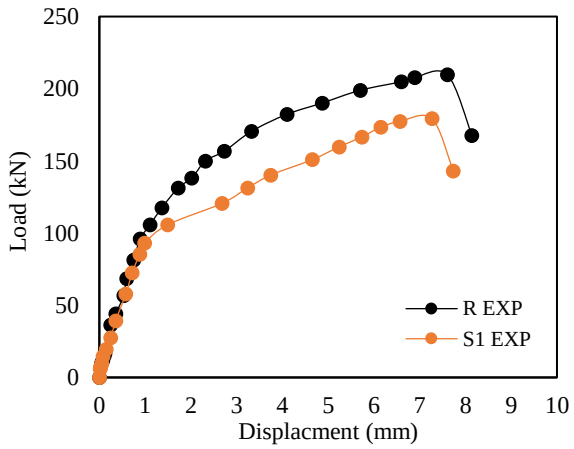

Figure 11. The load-displacement curve obtained from the loading test

To measure the slab angle after punching shear, the slabs were incised, and the reference points were used for measuring the punching shear angle on AA or BB sections (Figures 12b to 13b) by taking into account the punching shear failure intersection on the bottom surface of the slab and the outer edge of the column on the upper surface.

Next, the ideal model of the latest punching shear condition was plotted and fitted to the actual image of the laboratory concrete slab specimens. Figures 12b to 13b show the loading area with a yellow square, the critical results obtained from the experiment at the reinforcement level of the loaded slab model with a green curve (C), and the expansion of cracks with a red curve (D). The cracks are spread in the slabs through the cross-section of the steel rebar and the lower surface of the slab.

The slope of the developing critical shear cracks between the column edge and the reinforced bending surface was measured according to Figures 12b to 13b. Four points were selected at the reinforced bending surface for each slab with an effective depth (d) of 100 mm. Table 8 summarizes the related values. As it can be seen, the mean value of the points specified on the shapes is 21.6 cm, and the mean punching shear angle is 24.9 degrees. As Table 7 and Figures 12b to 13b demonstrate, it is concluded that the diameter of the punching cone in solid slab R is greater than that of void slab S_1; in addition, the location of the critical shear crack at the stress surface is on average 2.16d away from the edge of the column. The punching shear angle of the solid slab R cones is slightly smaller than that of the void slab S_1 cone.

3. NONLINEAR SLAB ANALYSIS

3. 1. Slab Modeling in Finite Element Software for both Soil and Spring Models ABAQUS was used to model the specimens assessed in the present study. In addition, the concrete damaged plasticity (CDP) model was used to model the slabs, which is a robust

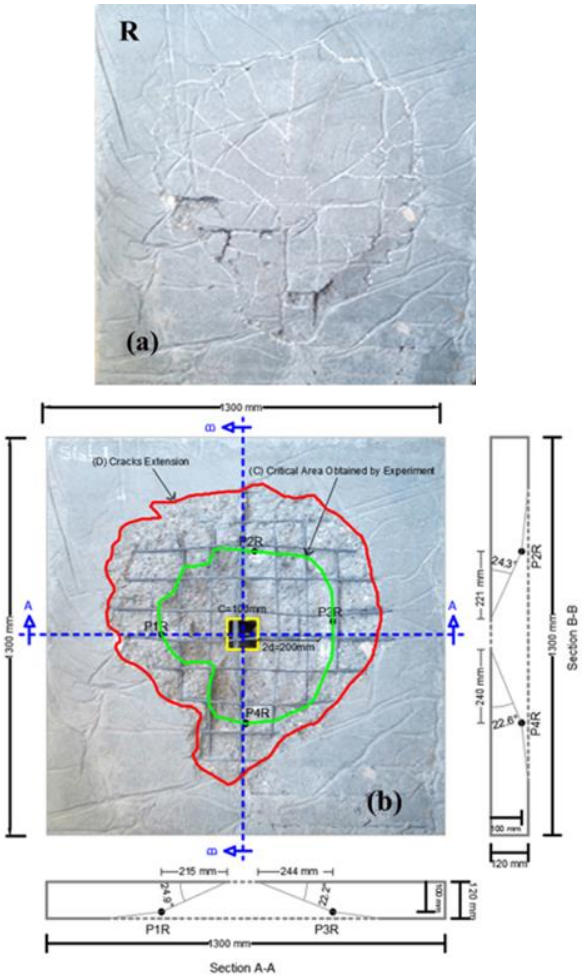

Figure 12. Slabs after punching shear: (a) specimen R before the autopsy; (b) specimen R after the autopsy and the measured punching shear angle

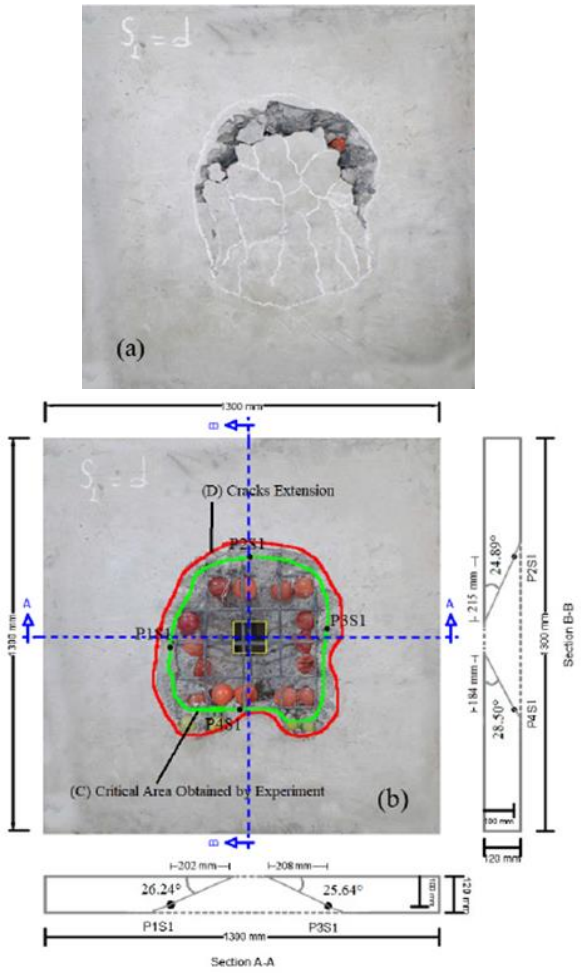

Figure 13. Slabs after punching shear: (a) specimen S_1 before the autopsy; (b) specimen S_1 after the autopsy and the measured punching shear angle

TABLE 7. The distance of shear cracks from the column edge and the mean crack distance from the column edge and punching inclination

Specimen	Values relative to the level of reinforcement				Average value for the distance of the crack from the column edge (mm)
	Marked points	Distance of the crack from the column edge (mm)	*In tension face	Angle of inclination (°)	
R	P1R	215	2.15d*	24.9	230
	P2R	221	2.21d	24.3	
	P3R	244	2.44d	22.2	
	P4R	240	2.40d	22.6	
S_1	P1S1	202	2.02d	26.2	202
	P2S1	215	2.15d	24.9	
	P3S1	208	2.08d	25.6	
	P4S1	184	1.84d	28.5	
Ave distance= 216 (mm)			Ave=2.16d	Ave failure angle=24.9	

*d = the effective depth of slab = 100 mm

*One could conclude that the critical shear crack site at the tension area is on average 2.16d away from the column edge, which is in general very close to EC2 [14]

model used for different loads to measure concrete behavior more accurately by expressing its distinct behavior under pressure and tension. In this model, the nonlinear behavior of concrete is expressed using the concepts of damaged isotropic elasticity as well as tensile and compressive plastics. To follow the simulation procedure more accurately, the mechanical properties of concrete, steel, and soil were entered into the software as shown inTables 2, 3, 5, and 8. According to Skorpen and Dekker [10], all constraints involved in these elements were entered into the software. The program used an average mesh size of 25 mm utilized an 8-node linear hexahedral solid element with a reduced integration (C3D8R) element for the solid slab concrete (R), soil, and the column. In addition, a 4-node tetrahedral (C3D4) element was used for the void slab (S1), and a 2-node linear truss (T3D2) was used to model the steel bars. Specimen R had 13520 mesh elements and 16854 nodes, specimen S1 contained 92110 mesh elements and 19230 nodes, the column had 160 mesh elements and 275 nodes, the soil had 40800 mesh elements and 45696 nodes, and the bars contained 52 mesh elements and 53 nodes. To model the springs, the linear model of Point to Ground was used, with a spring underneath each node.

Figure 14 shows the details of the geometry and boundary conditions of the specimens used for the simulations. Both slabs R and S1 were analyzed using the static method in the ABAQUS/Standard analyzer. In the static analysis, the load was applied perpendicular to the entire column surface, using the displacement control.

TABLE 8. CDP input data for concrete with $\acute{f}_c$=31.77 Mpa-Plasticity [9]

Dilatation Angle (◦)	Eccentricity	$F = \sigma_{b_0}/\sigma_{b_c}$	$K_c = \bar{q}_{TM}/\bar{q}_{cm}$	Viscosity Parameter
35	0.1	1.16	0.667	0.001

3. 2. Description of the Analyzed Specimens on the Soil and Springs To validate numerical models for measuring the punching shear capacity, finite element models (S1 and R) were simulated exactly similar to the corresponding laboratory specimens on the soil substrate and spring. However, to measure the soil spring constant for the spring support, various spring constants were investigated in Finite Element Software ABAQUS. For this purpose, 6 specimens of two-sided solid slabs were modeled and analyzed with springs placed 120 mm away from the column with different constants. After optimizing the spring constant and determining the soil-spring constant, a void slab with spherical void formers, placed 100 mm from the column, was modeled similar to the laboratory specimen, and then the punching shear capacity was evaluated numerically. In addition, the results of the punching shear capacity of the slabs on the soil substrate and springs were compared with those of the laboratory work. At the end, the failure mechanism of the modeled slabs in both supports (soil and springs) was compared with that of the laboratory specimens so that in case they matched each other, the results of finite element modeling would be considered reliable.

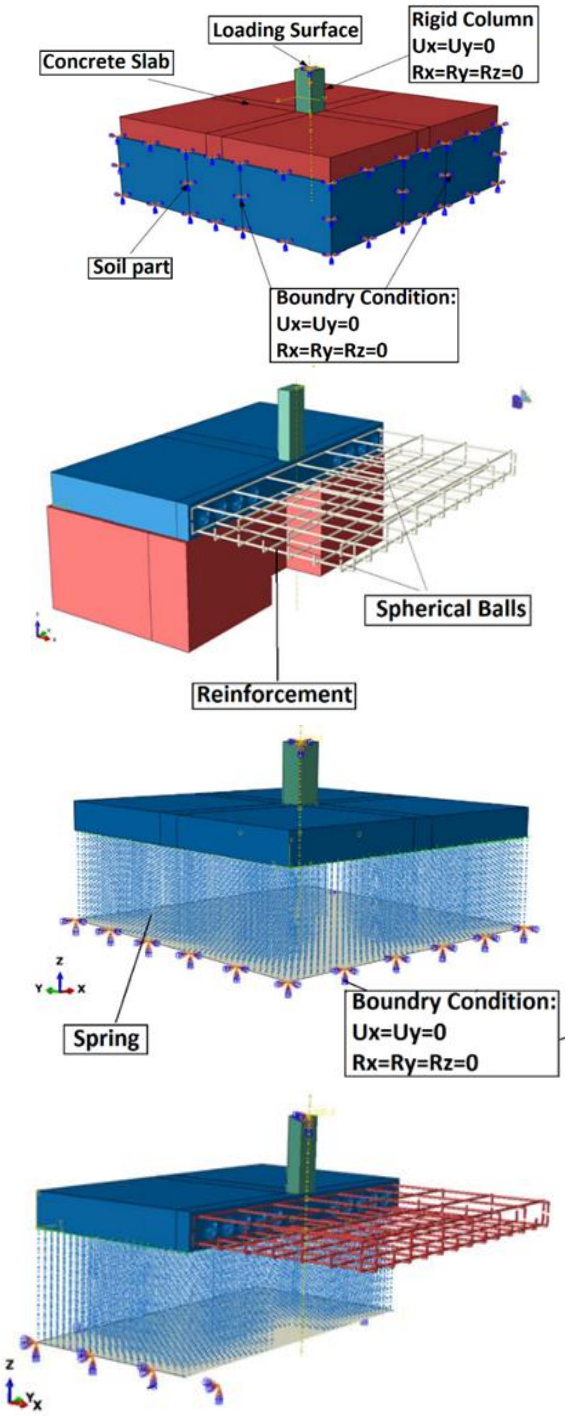

Figure 14. Introducing slab parts (geometry and boundary conditions) on the spring as the support and meshing of the finite element model for the concrete slab

4. NUMERICAL RESULTS

4. 1. Load-displacement Results of the Specimens Analyzed on Soil The numerical results of the final loads, load-displacement curves, and initial crack loads were compared with those of the experimental section. The comparison was performed for the purpose of numerical model validation. Table 9 demonstrates the results from the comparison of the experimental and numerical final loads for the models of the study. In addition, Table 10 depicts the comparison of the numerical and experimental results of the first cracking load for the solid and void slab models.

In general, the final loads predicted by the numerical analysis were heavier than the ones determined by the experiments. The differences in the final loads varied from 5.25 to 7.52% for both solid and void models, as Table 9 shows. The numerical data for all cases showed that the numerical values recorded for the soil and void models were higher than the experimental values with the difference of 10.48% and 8.17%, respectively.

According to the comparison results, the numerical models are stiffer; in addition, the numerical analysis demonstrates a lower value for deflection and a higher value for the final load with a slight difference in the final load values (see Figure 15). This could be due to four reasons; firstly, the concrete used in the experimental models was not fully homogeneous as assumed in the numerical models; secondly, the finite element model was inherently stiffer than the experimental specimen because of the reduced degrees of freedom in the elements; thirdly, the connection between the steel bars and the concrete slab was assumed to be completely continuous, with no slippage; and fourthly, since the elements representing the steel bars were modeled in longitudinal and transverse directions at the same height, there was a great deal of stiffness in the nodes where these elements intersected. However, there was no connection between the steel bars in the two directions in the laboratory specimen. Therefore, this method did not fully model the intersection points of the steel bars. As a result, the load-deflection response of the model had a steeper slope than the laboratory specimen.

TABLE 9. A comparison between experimental and numerical final loads

Slab Model Symbol	Ultimate Load Pu kN		Difference Ratio %
	Experimental	FEM	
R	209.72	220.73	5.25
S_1	179.34	192.83	7.52

TABLE 10. A comparison between the numerical and experimental results of the first cracking load

Slab Model symbol	1st Cracking Load kN		$\frac{Pcr)Num}{Pcr)Exp}$
	Experimental Pcr Exp.	Numerical Pcr *Num*	
R	96.04	106.11	1.10
S_1	85.26	92.23	1.08

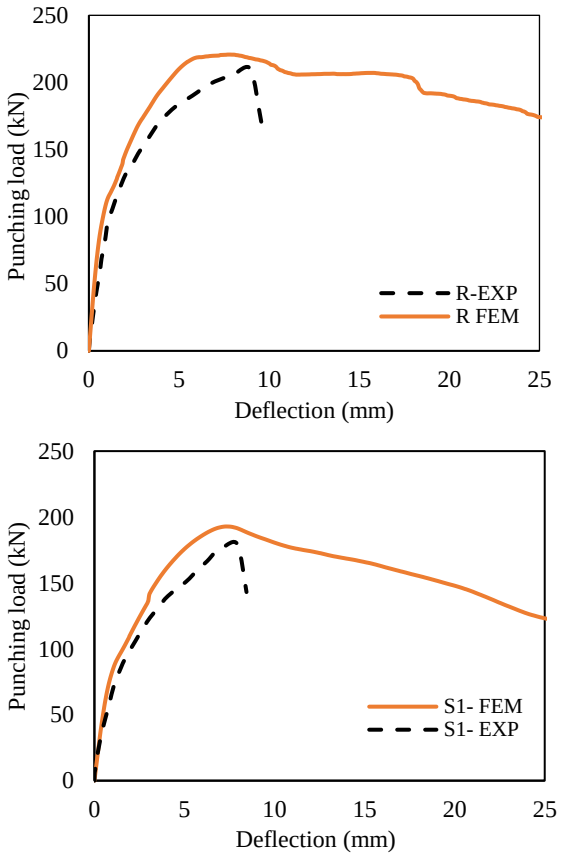

Figure 15. Loads versus central displacement curves

4. 2. Spring Stiffness Optimization and Slab Load-Deflection Evaluation To determine the soil-spring constant, 6 solid slab specimens were modeled and analyzed on the spring support, with the springs positioned 120 mm away from the column side. The analysis results are presented in the form of final load deflection in Table 11 as well as load deflection in Figure 16. As displayed in the final load-spring constant curve in Figure 17 as well as in the final deflection-spring constant curve in Figure 18, with an increase in the spring constant from 1000 to 6000 kN/m, the final load values increased and their corresponding deflection values decreased. Within the constant range of 4000-6000 kN/m, the displacement values and the final punching load were minimized and became fixed. As Figure 16 shows, the solid slabs generally exhibit the same behavior in the elastic zone so that they overlay roughly in the elastic zone of the solid slab on the soil substrate. Therefore, it could be concluded that the optimal spring constant is 5000 kN/m when the spring is placed at a distance of 120 mm from the column side.

Similar to the laboratory specimen, a numerical model was modeled and analyzed for the S1 void slab (Slab 7) under optimum constant conditions of the springs, Kopt = 5000 kN/m, where the springs were positioned at a distance of 120 mm from the column edge. The numerical values obtained for the final loads, displacement-load curves, and initial crack loads were compared with those of the experimental results. This comparison was performed to validate the numerical

TABLE 11. Different spring constants at three different distances from the edge of the column for optimizing the spring constant

Slab Model Symbol	Constant Springs (kN/m)	Punching Load (kN)	Deflection (mm)
Slab1	1000	182.18	9.00
Slab 2	2000	216.14	8.49
Slab 3	3000	220.10	8.14
Slab 4	4000	227.19	7.56
R-(Slab 5)	5000	235.10	7.55
Slab 6	6000	235.40	7.55

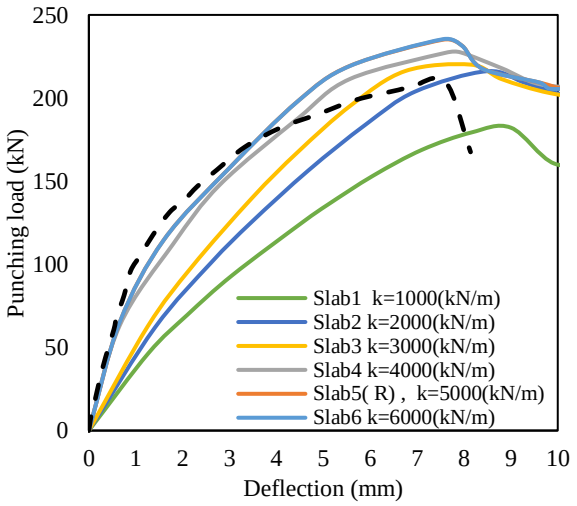

Figure 16. The comparison of load- deflection curves in two-way solid slabs with varying constant values at d=120 mm from the edge of the column

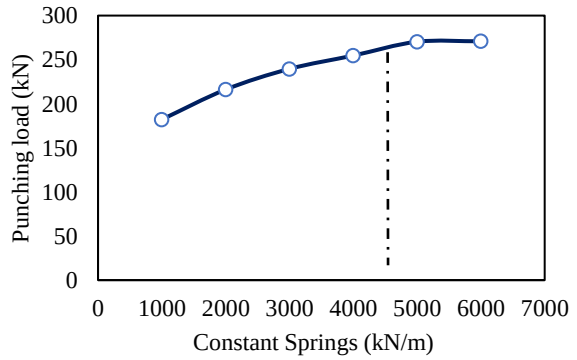

Figure 17. The ultimate deflection-spring constant diagram of the column edge for a two-way solid slab

model. Table 12 shows the comparison results of the experimental and numerical values of the final loads in the models of the study. Likewise, Table 13 demonstrates the comparison of the numerical and experimental results for the first load cracks in the slab and void models. The difference ratio of the final loads is 12.10% and 15.65% for the solid and void slabs, respectively, as Table 12 shows. The numerical data for all cases implied that the numerical values recorded for the soil and void models were higher than the experimental values, with the difference of 10.20% and 12.64%, respectively.

Figure 19 shows the results of the comparison made between the experimental and numerical values for the load versus the central displacement curves in the solid and hollow models on the spring support. The comparison results indicate that the use of numerical models is more difficult; in addition, the numerical analysis shows a lower value for deflection and a higher value for the final load, with a slight difference in the final load values.

4. 3. The fracture Mechanism of the Soil and Spring Specimens Figures 20 to 23 show the cracking patterns obtained from the finite element (FE) analysis. In numerical models, crack patterns are visualized using maximum plastic strains. According to the plastic strain counters, for the maximum main stress in the light blue areas where the strain is greater than 0.0015, the slab has reached its maximum puncture resistance. In infinite element models, the fracture mechanism is shown as a single slope, with the effective depth under the slab being 100 mm. Accordingly, the crack width, path, and shear fracture mode are plotted.

The crack width for the punching shear zone ranges from 198 to 231 mm for the hollow and solid slabs on the

TABLE 12. Experimental and numerical values of the final loads for solid and void slab models on the spring support

Slab Models Symbol	Ultimate Load Pu kN		Difference Ratio %
	Experimental	FEM	
R	209.72	235.10	12.10
S1	179.34	207.42	15.65

TABLE 13. Experimental and numerical values of the initial cracking loads for solid and void slab models on the spring support

Slab Model Symbol	1st Cracking Load kN		$\frac{Pcr)num}{Pcr)exp}$
	Experimental Pcr) exp.	Numerical Pcr) *num.*	
R	96.04	105.84	1.10
S1	85.26	96.04	1.12

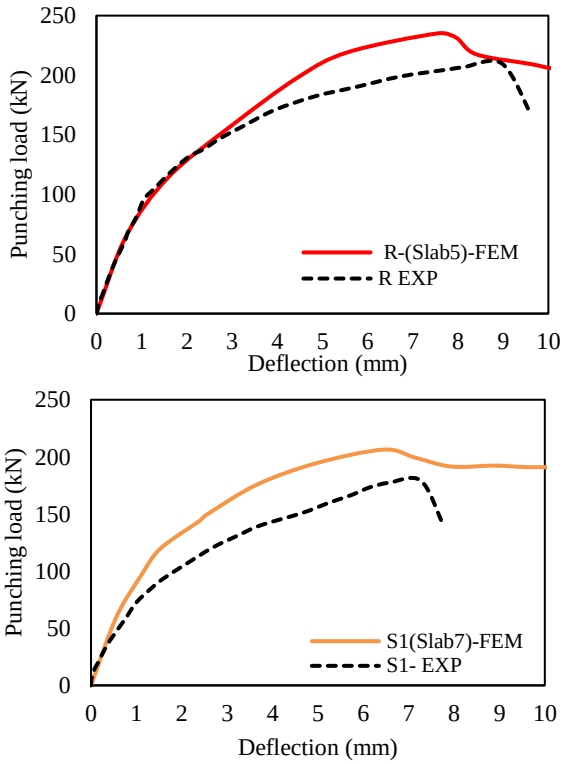

Figure 19. Deflection-load curves for solid and hallow models

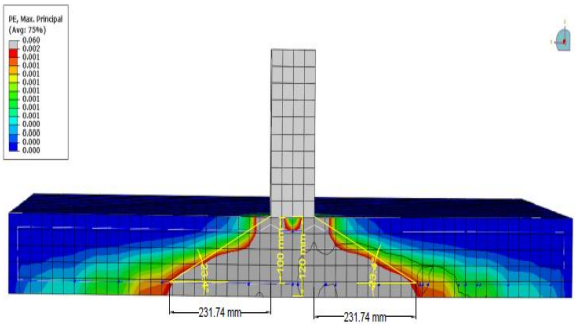

Figure 20. The fracture pattern for slab R (on the soil) at the final load under maximum plastic strains

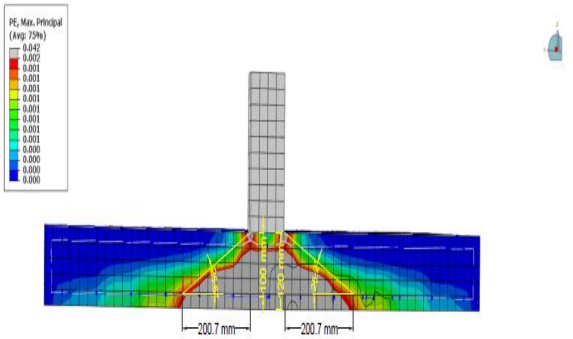

Figure 21. The fracture pattern for slab S1 (on the soil) at the final load under maximum plastic strains

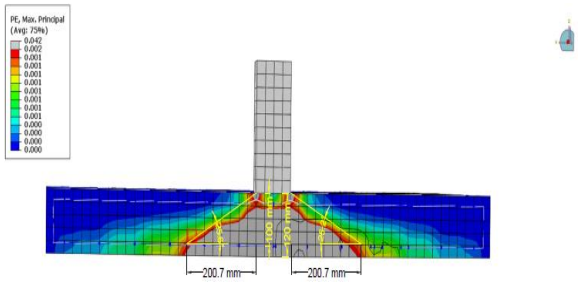

Figure 22. The fracture pattern for slab R (on the spring) at the final load under maximum plastic strains

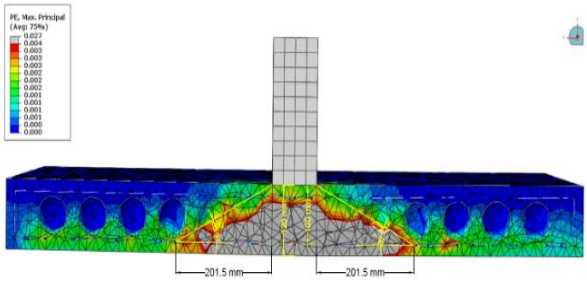

Figure 23. The fracture pattern for slab S1 (on the spring) at the final load under maximum plastic strains

soil, and from 200 to 201 mm for the hollow and solid slabs on springs. Besides, the angles of the diagonal fracture surface range from 26.2 to 23.4° for the slabs on the soil and 26.3 to 25.6° for the hollow and solid slabs on the spring as Table 14 shows.

Compared to the crack patterns in the experimental study, the proposed nonlinear model made an accurate prediction of crack propagation locations and directions. Figures 24 and 25 show the schemes of the final crack patterns for the slabs. The crack patterns in the laboratory experiments and those in the nonlinear models fit well. In general, the initial cracks appearing at the end of the elastic phase moved obliquely from the slab center to the slab edges.

TABLE 14. The crack width of the punching shear zone and the crack skew angle in the punching shear

Support Type	Specimen	Average Crack Angle	Distance of the Crack from the Column Edge (mm)
Soil-EXP	R	Ave (for 4 points) =23.5	230
Soil-FEM	R	23.4	23.1
Spring-FEM	R-(Slab5)	25.6	200
Soil-EXP	S1	Ave (for 4 points) =26.3	202
Soil-FEM	S1	26.2	198
Spring-FEM	S1-(Slab7)	26.3	201

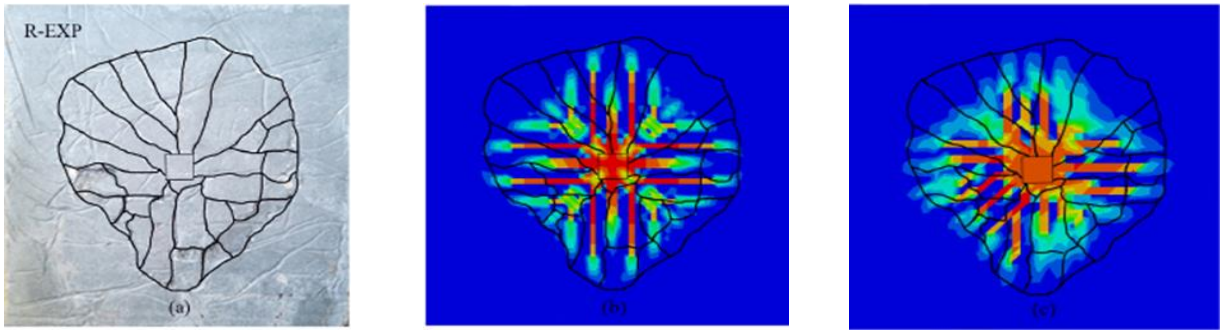

Figure 24. Crack patterns in (a) the laboratory experiment on specimen R, (b) nonlinear model R on soil, and (c) nonlinear mod springs

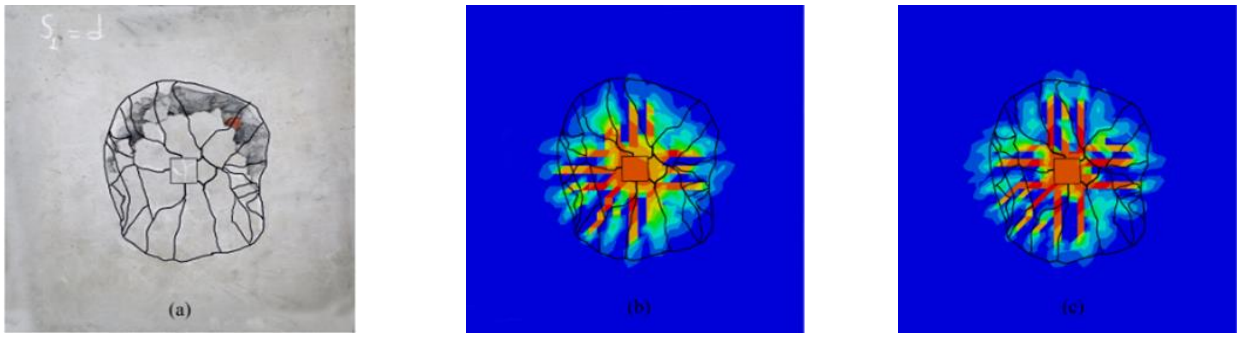

Figure 25. Crack patterns in (a) the laboratory experiment on specimen S_1, (b) nonlinear model S_1 on soil, and (c) nonlinear model S_1 on springs

5. CONCLUSION

Considering the results from the experimental data as well as the finite element analysis for the solid and hollow models of the study, the following conclusions were drawn:

- The solid and void slabs under analysis underwent a fracture due to the punching shear at 209.72 and 179.34 kN, respectively, at an average distance of 2.16d from the column circumference. The cracks in both slabs had irregular oval shapes that could be resulted from different performances of the materials, such as soil, concrete, and bars.
- In general, the first shear cracking for solid and void slabs started with 45.79 and 47.54% of the final load. Due to the presence of the balls, the final loads of the void slabs were smaller than those of the solid ones. The value of the punching shear resistance of the void slab was by 14.48% different from that of the solid slab.
- Vertical deflection (displacement or deformation) in the midpoint of the slabs, measured by the LVDT, was almost similar in both laboratory slabs, and deflection was not affected by the spherical balls until initial cracking.
- The cracking patterns in the experimental experiments and in nonlinear models were highly consistent. In general, the initial cracks appearing at the end of the elastic phase moved obliquely from the slab center to the slab edges.
- In general, the final loads predicted by the numerical analysis were heavier than those calculated in the laboratory experiments on the soil substrate and springs. Percentage differences in the final loads were 5.25% and 7.52% for the solid and hollow models, respectively, on the soil substrate. In addition, percentage differences for the final loads varied from 12.10 to 15.65% for both solid and hollow models on the springs.
- According to the experimental and numerical results, the punching shear strength of the slab model was higher than that of the void slab, and crack propagation in the former slab was higher than in the void slab.
- At the spring constant of 5000 kN/m, the solid slabs behaved similarly in the elastic zone until they roughly matched the elastic zone of the solid slab on the soil substrate and reached the soil spring constant.
- The 3D numerical analysis by ABAQUS showed that the actual behavior of the solid and void slab models on the soil and springs could be effectively simulated with a certain degree of accuracy. One of the main points in this analysis is the right choice of the modeling technique for the materials used.
- In the end, based on the findings explained above, it could be concluded that the uniformly-grained soil and springs could be reliable materials for the simulation of a uniformly distributed load, i.e. the dead load of the ceiling, applied to the column. Thus, the critical area of the punching shear is about 2d, which matches the Eurocode 2 (EC2).

6. REFERENCES

1. Dieterle, H., and Steinle, A. "Blockfundamente für Stahlbetonfertigstützen." Deutscher Ausschuss für Stahlbeton, Heft 387, Berlin, Germany, (1981). Retrieved from https://trid.trb.org/view/1032408 [German]
2. Dieterle, H., and Rostásy, F. "Tragverhalten quadratischer Einzelfundamente aus Stahlbeton." Deutscher Ausschuss für Stahlbeton, Heft 387, Berlin, Germany, (1987).
3. Hallgren, M., Kinnunen, S., and Nylander, B. "Punching Shear Tests of Column Footings." ***Nordic Concrete Research***, Vol. 21, (1998), 1–22. Retrieved from https://www.diva-portal.org/smash/record.jsf?pid=diva2:474585
4. Hegger, J., Sherif, A. G., and Ricker, M. "Experimental Investigations on Punching Behavior of Reinforced Concrete Footings - ProQuest." ***ACI Structural Journal***, Vol. 103, No. 4, (2006), 604–613. Retrieved from https://search.proquest.com/docview/198357965?pq-origsite=gscholar&fromopenview=true
5. Hegger, J., Ricker, M., Ulke, B., and Ziegler, M. "Investigations on the punching behaviour of reinforced concrete footings." ***Engineering Structures***, Vol. 29, No. 9, (2007), 2233–2241. https://doi.org/10.1016/j.engstruct.2006.11.012
6. Hegger, J., Ricker, M., and Sherif, A. "Punching strength of reinforced concrete footings." ***ACI Structural Journal***, Vol. 107, No. 4, (2010), 494–496.
7. Bonić, Z., and Folić, R. "Punching of column footings - Comparison of experimental and calculation results." ***Gradjevinar***, Vol. 65, No. 10, (2013), 887–899. https://doi.org/10.14256/jce.916.2013
8. Falkner, H., and Teutsch, M. "Comperative investigations of plain and steel fibre reinforced industrial ground slabs." Institut Fur Baustoffe, Massivbau und Brandschutz, (1993).
9. Jankowiak, T., and Łodygowski, T. "Identification of parameters of concrete damage plasticity constitutive model." ***Foundations of Civil and Environmental Engineering***, Vol. 6, (2005), 53–69. Retrieved from https://www.infona.pl/resource/bwmeta1.element.baztech-article-BPP1-0059-0053
10. S A Skorpen, and N W Dekker. "The application and interpretation of linear finite element analysis results in the design and detailing of hogging moment regions in reinforced concrete flat plates." ***Journal of the South African Institution of Civil Engineering***, Vol. 56, No. 1, (2014), 77–92. Retrieved from http://www.scielo.org.za/scielo.php?script=sci_arttext&pid=S1021-20192014000100009
11. Abaqus Theory Manual (6.14). Dassault Systemes, Providence, RI, USA, 2014.
12. Valivonis, J., Skuturna, T., Daugevičius, M., and Šneideris, A. "Punching shear strength of reinforced concrete slabs with plastic void formers." ***Construction and Building Materials***, Vol. 145, (2017), 518–527. https://doi.org/10.1016/j.conbuildmat.2017.04.057
13. Eurocode 2: Design of Concrete Structures-Part 1-1. General rules and rules for buildings. BS EN 1992-1-1, 2004: 97–105.
14. Ozturk, B. "Free vibration analysis of beam on elastic foundation by the variational iteration method." ***International Journal of Nonlinear Sciences and Numerical Simulation***, Vol. 10, No. 10,

(2009), 1255–1262. https://doi.org/10.1515/IJNSNS.2009.10.10.1255

15. Ozturk, B., and Coskun, S. B. "The Homotopy Perturbation Method for free vibration analysis of beam on elastic foundation." ***Structural Engineering and Mechanics***, Vol. 37, No. 4, (2011), 415–425. https://doi.org/10.12989/sem.2011.37.4.415
16. Ozturk, B., and Coskun, S. B. "Analytical solution for free vibration analysis of beam on elastic foundation with different support conditions." ***Mathematical Problems in Engineering***, Vol. 2013, , (2013). https://doi.org/10.1155/2013/470927
17. Zhang, W. X., Li, B., Hwang, H. J., Zhang, J. Y., Xiao, L. J., Yi, W. jian, and Park, H. G. "Punching shear strength of reinforced concrete column footings under eccentric compression: Experiment and analysis." ***Engineering Structures***, Vol. 198, (2019), 109509. https://doi.org/10.1016/j.engstruct.2019.109509

Persian Abstract

چکیده

در این تحقیق به منظور بررسی برش منگنه‌ای در دال‌های مجوف و توپر و شبیه‌سازی مدل خاک و فنر به عنوان بار گسترده بر روی این دالها، با آنالیز المان محدود غیرخطی این دال‌ها تحت بارگذاری استاتیک برای بررسی حالت خرابی آن‌ها از نظر بار نهایی و الگوهای ترک خوردگی روی بستر خاک و فنر انجام شد. آنالیز المان محدود سه بعدی با مدل‌سازی مناسب از لحاظ سایز المان، مش و مدل‌سازی مشخصه بتن انجام شد. در نرم‌افزار المان محدود ABAQUS 6.19، رفتار غیرخطی مصالح ترد براساس مدل آسیب‌دیدگی بتن (CDP) تعریف شد. نتایج آنالیز عددی دالها بر اساس مقایسه با نمونه‌های تجربی روی بستر خاک در همین تحقیق کالیبره و صحت‌سنجی شدند. در نهایت با بهینه نمودن ثابت فنر و رسیدن به ثابت فنر خاک، جهت صحت سنجی نتایج آنالیز عددی دالها روی تکیه‌گاه فنر با نتایج تجربی مقایسه گردید. مقایسه بین نتایج تجربی و عددی نشان می‌دهد که مدل‌های کالیبره شده به درستی پاسخ برش منگنه‌ای دالها را پیش‌بینی می‌کند و می‌توان فنر را به عنوان بار گسترده یکنواخت (بار مرده) در مدل‌سازی بکار برد.